



Materials subjected to fast neutron irradiation/Matériaux soumis à irradiation par neutrons rapides

## Fissile core and Tritium-Breeding Blanket: structural materials and their requirements

Jean-Louis Boutard<sup>a,\*</sup>, Ana Alamo<sup>b</sup>, Rainer Lindau<sup>c</sup>, Michael Rieth<sup>c</sup>

<sup>a</sup> EFDA-CSU Garching, Boltzmannstrasse 2, 85748 Garching bei München, Germany

<sup>b</sup> DEN/DSOE, CEA/Saclay, 91191 Gif-sur-Yvette cedex, France

<sup>c</sup> IMF-1 FZK, Hermann-von-Helmholtz Platz 1, 76344 Eggenstein-Leopoldshafen, Germany

Available online 7 March 2008

### Abstract

High radiation resistant structural materials for fusion and fission nuclear power plants are a key issue for the development of both types of reactors. Selection criteria, elements of metallurgy of the selected materials, and the major issues as they are revealed by the results of the present development programmes, are presented. At low temperature ( $\sim 300^\circ\text{C}$ ) ferritic/martensitic steels are suffering from He-embrittlement, associated with possible hardening due to  $\alpha/\alpha'$  unmixing. The kinetics of hardening and embrittlement versus dose, especially saturation with dose, are still open key issues, difficult to settle on the basis of a purely experimental programme. Important progress is still to be made in mastering the initial microstructure, inclusion cleanliness and joining techniques of oxide dispersion strengthened steels for higher heat resistance. Physics modeling as presented in this issue should promote guidance to the understanding of the mechanisms involved, provide solutions to master the initial microstructure and phase stability, and mitigate the in-service property degradation. **To cite this article: J.-L. Boutard et al., C. R. Physique 9 (2008).**

© 2007 Published by Elsevier Masson SAS on behalf of Académie des sciences.

### Résumé

**Cœur fissile et couverture tritigène : les matériaux de structure et leurs spécifications.** Des matériaux ayant une excellente résistance aux effets d'irradiation sont indispensables au succès des futures centrales de fission et de fusion. On présente les critères de sélection, les éléments caractéristiques de la métallurgie et les principaux effets d'irradiation révélés par les programmes d'irradiation des matériaux retenus. A basse température ( $\sim 300^\circ\text{C}$ ) les aciers ferritiques/martensitiques souffrent de fragilisation par l'hélium associée à un probable durcissement dû à la décomposition  $\alpha/\alpha'$ . Les cinétiques de durcissement et de fragilisation et tout particulièrement la saturation avec la dose sont des questions difficiles à trancher sur la seule base d'un programme expérimental. Des progrès importants sont encore nécessaires pour maîtriser la microstructure, la propreté inclusionnaire et l'assemblage des aciers renforcés par dispersion d'oxydes. Une modélisation physique telle que présentée dans ce volume doit servir de guide pour comprendre les mécanismes et fournir des solutions pour limiter la dégradation des propriétés en service. **Pour citer cet article : J.-L. Boutard et al., C. R. Physique 9 (2008).**

© 2007 Published by Elsevier Masson SAS on behalf of Académie des sciences.

**Keywords:** Structural materials; Ferritic/Martensitic steels; Ferritic steels;  $\text{SiC}_f/\text{SiC}$  composites; Radiation effects

\* Corresponding author.

E-mail address: [jean-louis.boutard@tech.efda.org](mailto:jean-louis.boutard@tech.efda.org) (J.-L. Boutard).

## 1. Introduction

Future thermo-nuclear fusion and Generation IV fission Nuclear Power Plants (NPPs) should provide mankind with sustainable energy sources with a low release of green-house effect gases, which could contribute to the energy mix required to satisfy the growing demand for energy and to limit the global warming of our planet.

The decision to construct the International Thermo-Nuclear Reactor (ITER) taken by China, the European Union (EURATOM), India, Japan, Korea, Russia and the USA is the essential step towards knowledge of the physics of thermo-nuclear plasmas for the future fusion NPPs, the reliable and economic operation of which will also require the development of materials and components able to resist irradiation by the 14 MeV neutrons from the deuterium-tritium fusion. Similarly radiation resistant structural materials will be required for a successful development of the fast neutron reactors being studied by Brazil, Canada, France, Korea, South Africa, Switzerland, United Kingdom and the United States within the Gen IV International Forum (GIF).

This article will present the requirements for the structural materials highly irradiated in both types of NPP, the main characteristics of their metallurgy, and the most important experimental results concerning their radiation effect resistance. In Section 2 some essential principles of fusion and fission NPPs are succinctly presented. Section 3 gives design concepts with operating conditions and structural materials selected for the Tritium-Breeding Blankets and fissile cores of fusion and fast reactors, respectively. Section 4 details the selection criteria and elements of the metallurgy of the chosen materials. Section 5 describes the main experimental results concerning radiation effects under fusion and fission spectra. In Section 6 some elements of conclusion are given in strategic terms for an effective and reliable development of highly resistant structural materials for fusion and fission applications.

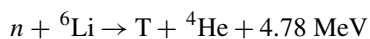
## 2. Thermo-nuclear fusion and fast neutron NPPs

In a fusion NPP the energy will be produced by the fusion reaction between deuterium (D) and tritium (T) nuclei:



As a consequence, 80% of the fusion energy is carried by the 14 MeV neutrons and 20% by the 3.6 MeV alpha particles. In order to have a significant effective cross section for this reaction, the D and T nuclei must have a sufficiently high kinetic energy or temperature of the order of  $100 \times 10^6$  K. Such kinetic energies will be obtained in magnetically confined hot plasmas. In addition, for a fusion NPP, the thermo-nuclear plasma has to meet the condition of self-sustained ignition i.e. have an energy relaxation time  $\tau_E$ , an electronic density  $n$ , and a temperature  $T$  high enough so that  $nT\tau_E > 5 \times 10^{21} \text{ m}^{-3} \text{ keV s}$ . The magnetic configuration to meet these conditions will be most probably of Tokamak type [1], as in most of the present physics machines and ITER.

Two in-vessel components are particularly important: the divertor and the Tritium-Breeding Blankets (TBB). The divertor is essential for a self-sustained ignition: it (i) purifies the plasma by locally creating a magnetic configuration to evacuate the alpha particles and impurities, and (ii) extracts a significant part of the produced fusion energy. The TBB requirements are three-folds. They first extract the fusion energy. Secondly, as the half life time of tritium is only  $\sim 12$  years, tritium almost does not exist on the Earth and TBBs have to produce it for a self-sufficient operation. The following nuclear reaction between the D–T fusion neutrons and the  ${}^6\text{Li}$  nuclei is used:



The energy to be extracted by the TBB is deposited by the 14 MeV neutrons along their trajectory and released by the nuclear reaction producing the tritium. For tritium self-sufficiency every D–T fusion neutron has to be used to produce at least one tritium atom. Neutron multiplier functional materials such as Pb or Be are also introduced in the TBBs to compensate the unavoidable losses of neutrons resulting, for instance, from transmutation reactions. Last but not least, TBBs contribute to the shielding of the vacuum vessel and of the superconducting magnets of the Tokamak.

In the moderated neutron spectrum of the present water cooled fission NPPs the energy is produced by the fission of the  ${}^{235}\text{U}$  nuclei, which represent only 0.07% of natural uranium. Among the various concepts studied within the GIF [2], the Na or He-cooled fast reactors could contribute to a sustainable development of nuclear energy based on

fission, as they allow an optimized resource management and a strong reduction of waste [3]. In a fast spectrum, with neutron energy in the range of a few MeV, the isotope  $^{238}\text{U}$ , i.e. more than 99% of natural uranium, can be transmuted into  $^{239}\text{Pu}$ , which is easily fissile. In addition, the minor actinides such as  $^{237}\text{Np}$ ,  $^{241}\text{Am}$  and  $^{243}\text{Am}$  or  $^{243}\text{Cm}$ ,  $^{244}\text{Cm}$  and  $^{245}\text{Cm}$ , which are produced by successive neutron captures by U and Pu nuclei, can be transmuted by the fast neutron spectrum, allowing a strong reduction in volume and radioactivity of the nuclear waste.

### 3. Tritium-Breeding Blankets and fuel elements

Several design concepts are being envisaged for the TBBs based on: (i) solid lithium ceramics cooled either by water or helium with Be as neutron multiplier, and (ii) liquid lead lithium eutectic within a dual-coolant or He-cooled concept [1].

In all the design concepts of TBB the structural materials close to the First Wall (FW) will be subjected to high radiation effects due to the 14 MeV neutrons, resulting in 30 to 80 dpa (Displacements Per Atom) for the first Demonstration (DEMO) reactor or even 100 to 150 dpa for a first prototype NPP [4]. Simultaneously, the 14 MeV neutrons will produce significant concentrations of He and H, respectively  $\sim 10$  and  $\sim 45$  apm/dpa for the parts close to the FW in front of the plasma. The FW itself will have also to evacuate a peak heat flux  $\sim 0.5 \text{ MW/m}^2$ .

Fig. 1 presents the dual-coolant TBB concept, with the calculated operating temperatures and foreseen materials. The liquid Pb–Li eutectic is used as neutron multiplier (Pb) and as tritium breeding material (Li). It also contributes, with the helium gas, to the cooling of the TBB. The foreseen structural material is the reference Reduced Activation Ferritic-Martensitic (RAFM) steel EUROFER with an upper operation temperature limit of  $\sim 550 \text{ }^\circ\text{C}$ . Oxide Dispersion Strengthened (ODS) EUROFER is foreseen to be used as a FW plate, protected with W-tiles (not shown) facing the plasma, which will have to sustain operating temperatures up to  $700 \text{ }^\circ\text{C}$ . Inserts made of  $\text{SiC}_f/\text{SiC}$  composites are envisaged in the Pb–Li channels to: (i) thermally insulate and protect the martensitic steel EUROFER from too high operating temperatures, and (ii) act as low electrical conductivity material to limit electrical current loops through the metallic structure and thus mitigate the Magneto-Hydrodynamic effects within the liquid metal Pb–Li.

In addition to the 14 MeV neutron irradiation, the divertor will have to withstand a peak heat flux of  $\sim 10 \text{ MW/m}^2$ . The He-cooled concept foreseen for DEMO is a complex component made of ODS structural steels, refractory pro-

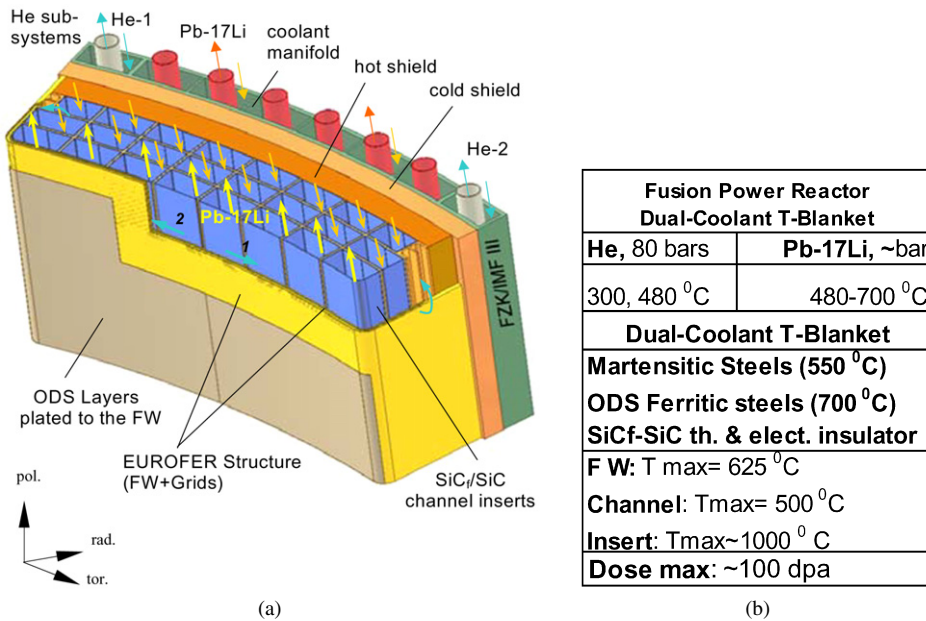


Fig. 1. (a) Schematic view of the dual-coolant concept of TBB with the selection of structural and functional materials. (b) Operating temperature ranges, pressure and inlet & outlet temperatures of the He coolant and of the Pb–Li eutectic [1].

Fig. 1. (a) Vue schématique du concept doublement refroidi de Couverture Tritigène (CT) avec indication des matériaux fonctionnels et de structure sélectionnés. (b) Intervalle des températures de service, pression et températures d'entrée et de sortie du caloporteur hélium ainsi que de l'eutectique Pb–Li [1].


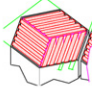

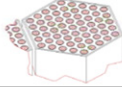
	GFR	SFR
<b>Coolant</b>	He, 70 bars	Liquid Na, a few bars
<b>In-&amp;-Outlet Temperature</b>	488, 850°C	380, 550°C
<b>Fuel element</b>	<b>GFR: (UPu)C pellets in plates in hexagonal sub-assembly</b>	
		
	<b>SFR: (UPu)O<sub>2</sub> pellets in cladding and hexagonal sub-assembly</b>	
		
<b>Core Structure</b>	<b>SiC composite</b>	<b>Martensitic Steels</b>
<b>Temperature</b>	600-1200°C->1650°C (incid.)	480-700°C
<b>Dose</b>	60/90 dpa	200 dpa
<b>Vessel</b>	9Cr martensitic steel (T91) or improved version (T92)	316L Austenitic steels

Fig. 2. Elements of design, structural materials and operating conditions for the fuel element of two fast reactors concepts of Gen IV: He-cooled and Na-cooled [3,7].

Fig. 2. Eléments de conception, matériaux de structure et conditions de service de l'élément combustible des deux concepts de réacteur rapide de Génération IV : refroidi à l'hélium et refroidi au sodium [3,7].

ductive  $W$  and heat sink and structure  $W$ -alloys selected, respectively, for a low sputtering rate in front of the plasma, high thermal conductivity and strength as well as potential radiation resistance [5], although  $W$ -alloys are known to suffer from initial low fracture toughness [6].

The fissile core of the He or Na-cooled fast reactors consists in a close-packed array of hexagonal sub-assemblies. Fuel element concepts, structural materials and operating conditions are summarized in Fig. 2 [3,7]. In the Na-cooled fast reactors the cladding material of the fuel element will have to undergo temperatures from 350 to 700 °C in nominal conditions and dose up to 200 dpa. ODS ferritic steels have been selected due to their high creep strength and high resistance to swelling. The material of the hexagonal tube, which is wrapping every sub-assembly, will have also to be as radiation resistant as the cladding material. Due to a lower maximum temperature  $\sim 500$ – $550$  °C, conventional 9Cr–1Mo (9Cr–1Mo–VNb) ferritic/martensitic steel has been selected. For the higher operating temperatures of the He-cooled fast reactor, both in nominal and incidental conditions, refractory ceramic composite materials of  $\text{SiC}_f/\text{SiC}$  type formed by an architecture of SiC fibres embedded in a SiC matrix have been chosen, on the basis of the excellent behaviour of the TRISO fuel particle of the High Temperature Reactor (HTR), which was made of successive coatings of pyrolytic carbon, chemical vapour deposited SiC and pyrolytic carbon around the fissile kernel [8].

The structural steels of the vessels of fusion and fission NPPs do not belong to the class of highly irradiated materials considered in this article. The 316L type austenitic steel and welds of the vessel of Na-cooled fast reactors show limited degradation of the mechanical properties under long term exposure at  $\sim 400$  °C up to a dose  $\sim 0.1$  dpa [9]. This article will amply demonstrate that the mod 9%Cr–1Mo ferritic/martensitic selected for the pressure vessel of the He-cooled fast reactors will undergo extremely limited degradation of its properties when maintained in the range 400–450 °C up to 0.1 dpa, although very long term thermal ageing driven microstructure evolution cannot be excluded during the sixty year lifetime of the vessel [10]. The foreseen 316L vacuum vessel of the DEMO reactor is still in the conceptual phase of definition, with the objective of having as low as possible in-service degradation of the mechanical properties of the base metal and welds.

#### 4. Selection criteria and elements of metallurgy

The properties of any material are controlled by its crystalline structure, chemical composition and microstructure. The displacement cascades induced by the Primary Knocked-on Atoms (PKA) produced by the bombardment of fast neutrons [11] destroys locally the crystalline structure. The surviving point defects will diffuse and agglomerate, eventually with helium in the case of fusion. A new microstructure is created, inducing hardening [12]. Possible

Table 1

Typical chemical compositions (in mass%) and metallurgical conditions of some representative ferritic and F/M steels. As, Sn, Sb, S and P have also to be strictly controlled to get rid of possible embrittlement in the initial condition. EUROFER is a Reduced Activation steel. The radiologically undesired elements have been measured in the following ranges given in ppm mass for ten heats corresponding to eleven tonnes and different product forms: Nb (2–7), Mo (10–32), Ni (70–280), Cu (15–220), Al (60–90), Ti (50–90), Si (400–700), Co (30–70). The Low Activation Requirements are: Nb < 0.01 ppm mass, Mo < 1, Ni < 10, Cu < 10, Al < 1, Ti < 200, Si < 400, Co < 10 [17]

Tableau 1

Compositions chimiques typiques (en % masse) et états métallurgiques de quelques aciers ferritiques et ferritiques/martensitiques. As, Sn, Sb, S et P doivent être strictement contrôlés pour éviter toute fragilisation à l'état initial. EUROFER est un acier à activation réduite. Les teneurs des éléments radiologiquement indésirables ont été mesurées et sont dans les intervalles suivants (en ppm masse) : Nb (2–7), Mo (10–32), Ni (70–280), Cu (15–220), Al (60–90), Ti (50–90), Si (400–700), Co (30–70). Les spécifications pour avoir un acier basse activation sont : Nb < 0.01 ppm masse, Mo < 1, Ni < 10, Cu < 10, Al < 1, Ti < 200, Si < 400, Co < 10 [17]

	C	Cr	Mo	Mn	Si	Ni	V	Nb	W	Ta	N	Metallurgical condition
F17 [15,16]	0.06	17.3	–	0.4	0.35	0.09	–	–	–	–	0.032	Recrystallized $\delta$ -ferrite
Mod 9Cr–1Mo [15,16]	0.11	8.3	0.95	0.38	0.43	0.13	0.2	0.08	–	–	0.02	Tempered martensite
Manet II [17]	0.11	10.3	0.61	0.78	–	0.68	0.2	0.14	–	–	0.031	Tempered martensite
12 Cr [15,16]	0.19	12.0	0.96	0.6	0.42	0.56	0.3	–	0.54	–	0.06	Tempered martensite
F–82H [17]	0.09	7.7	–	0.16	–	–	0.16	–	1.94	0.02	0.06	Tempered martensite
OPTIFER [17]	0.12	9.48	–	0.39	–	–	0.245	–	0.985	0.061	0.0225	Tempered martensite
EUROFER [17]	0.12	8.9	0.0015	0.47	0.06	0.022	0.2	0.0022	1.07	0.14	0.018	Tempered martensite

swelling can also occur: the surplus of surviving vacancies due to the preferential absorption of interstitials by the dislocation cores, clusters into cavity nuclei stabilized by the presence of gas [13]. Helium, itself, will strain the chemical bond due to its high solution energy [14].

#### 4.1. EUROFER and ferritic/martensitic steels

Ferritic and Ferritic/Martensitic (F/M) steels have been selected as structural materials for TBBs and fissile cores on the basis of the experience gained in the various Fast Breeder Reactors from the 1970s to now-a-days. Typical chemical compositions of 17% Cr ferritic and 9 and 12% Cr F/M steels are given in Table 1. These steels, extensively irradiated in Fast Breeder Reactors, exhibit no swelling at doses as high as 150 dpa in the temperature range 400–550 °C [15]. This behaviour is in contrast to austenitic steels, which exhibit swelling rates up to 1% per dpa, after an incubation dose generally smaller than  $\sim 100$  dpa [15]. In addition, conventional 9%Cr–1Mo showed very low embrittlement under irradiation within fast breeder reactors in the temperature range 400–550 °C [16].

For fusion reactors, tailored chemical compositions were developed to have Reduced Activation (RA) materials that can be recycled hands-on after  $\sim 100$  years following the end of life of the components, as shown in Fig. 3 [17]. For this purpose the carbide forming elements such as Mo or Nb are undesirable. They are replaced by W and Ta. Alloying elements or impurities such as Ni, Cu, Co, Ag or Al are also kept as low as possible to comply with low activation requirements (see Table 1). The developed RA 9%Cr–V–W–Ta F/M steels have mechanical and physical properties very similar to the classical modified 9%Cr–1Mo (9Cr–1MoVNb) F/M steel [18].

Although ferritic and F/M steels have the same Body-Centred Cubic (bcc) crystalline structure they have very different microstructures due to the phase diagram of the Fe–Cr system. The ferritic steels, due to high Cr content, keep their bcc crystalline structure up to the melting temperature. They have therefore a bcc crystalline structure during the solution-annealing treatment, and are given a final recrystallization temperature to obtain the recrystallized  $\delta$ -ferrite microstructure. For the F/M steels the crystalline structure is Face-Centred Cubic (fcc) during the austenitising heat-treatment at  $\sim 1000$  °C, the objective of which is to solution-anneal the alloying elements. The martensitic transformation occurs during the quenching down to room temperature via a shearing process of the fcc structure to a body tetragonal centred crystalline structure, the octahedral interstitial sites of which are occupied by carbon or nitrogen atoms [19]. The associated microstructure consists of laths with a very high density of dislocations, which is extremely hard (and brittle) as shown on Fig. 4(a). A tempering treatment has to be given, which results in: (i) the precipitation of the various carbides in a matrix of bcc crystalline structure, the  $\alpha$ -ferrite, and (ii) a partial recovery of the dislocation network. Fig. 4 shows that, depending on the temperatures of the austenitising and tempering heat-treatments, the final yield and Ductile-to-Brittle Transition Temperature (DBTT) can be varied on a large range:

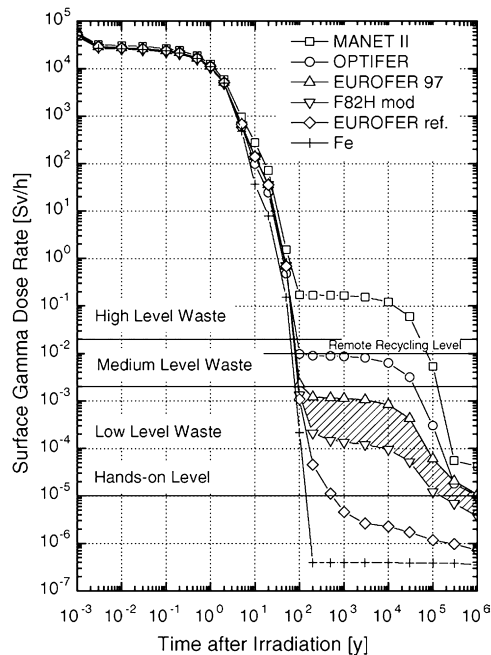


Fig. 3. Calculated decay of gamma surface dose rate in iron and F/M steels after irradiation up to 115 dpa equivalent to 12.5 MWyear/m<sup>2</sup> in a FW DEMO spectrum [17]. Chemical compositions of the various steels are given in Table 1 for the major alloying elements with restriction on the undesirable elements due to their activation given in the caption.

Fig. 3. Calcul de la décroissance de la dose de rayonnement gamma au contact d'échantillons de fer et d'aciers ferritiques/martensitiques irradiés à 115 dpa en position de première paroi de DEMO soit un équivalent de 12.5 MWyear/m<sup>2</sup> [17]. Les compositions chimiques des divers aciers considérés sont données dans le Tableau 1 pour les éléments d'alliage, et, dans la légende de ce même tableau pour les éléments radiologiquement indésirables.

austenitising at 950–1000 °C and tempering at ~750 °C allow for an acceptable compromise between strength and fracture toughness [20,21].

#### 4.2. ODS ferritic and ferritic/martensitic steels

In order to improve the creep strength of 9% Cr F/M steels above 550 °C, a world wide effort is being carried out. A first approach typical of the power generation application is based on optimizing the chemical compositions and heat-treatments of the conventional steels [22,23]. The second approach relies on developing ODS steels [24]. The heat resistance of optimized 9–12% F/M steels has been increased to ~600 °C. Nevertheless, 650 °C might be an upper limit within this approach. Conversely ODS F/M steels have heat resistance up to ~650 °C and ODS ferritic steels are capable of withstanding operating temperatures up to ~750 °C. Fig. 5 represents, versus the usual Larson–Miller (LM) parameter, the creep rupture stress of EUROFER, ODS-EUROFER and various ODS ferritic steels [25,26]. The ranges of times to rupture explored in these creep tests are similar for these materials. Therefore data points with higher LM parameters correspond to materials with higher heat resistance.

European development of ODS ferritic steels for the fast reactor cladding began in SCK.CEN/Mol in the late 1960s [27]. ODS steels are presently being developed for fission and fusion applications in Japan [28,29], in the Europe Union [30,31] and in the United States [25,32–34]. Table 2 gives typical chemical compositions of these ferritic steels [25,33,34]: 12Y1, 12YWT and 14YWT are laboratory batches developed by ORNL; MA956, MA957 and PM2000 are industrial grades. MA956 and 957 were developed by International Nickel Company (INCO), PM2000 by Metallwerk Plansee. A high density of nano-sized obstacles is the major element, which controls the high creep strength of ODS steels

The initial step in the fabrication of ODS steels consists in Mechanical Alloying (MA) the elementary or pre-alloyed powders of the metallic matrix complemented with the adequate quantity of yttria (Y<sub>2</sub>O<sub>3</sub>) powder. During MA, the alloy is subjected to repeated forcing events, energetic collisions between balls and the powder particles,

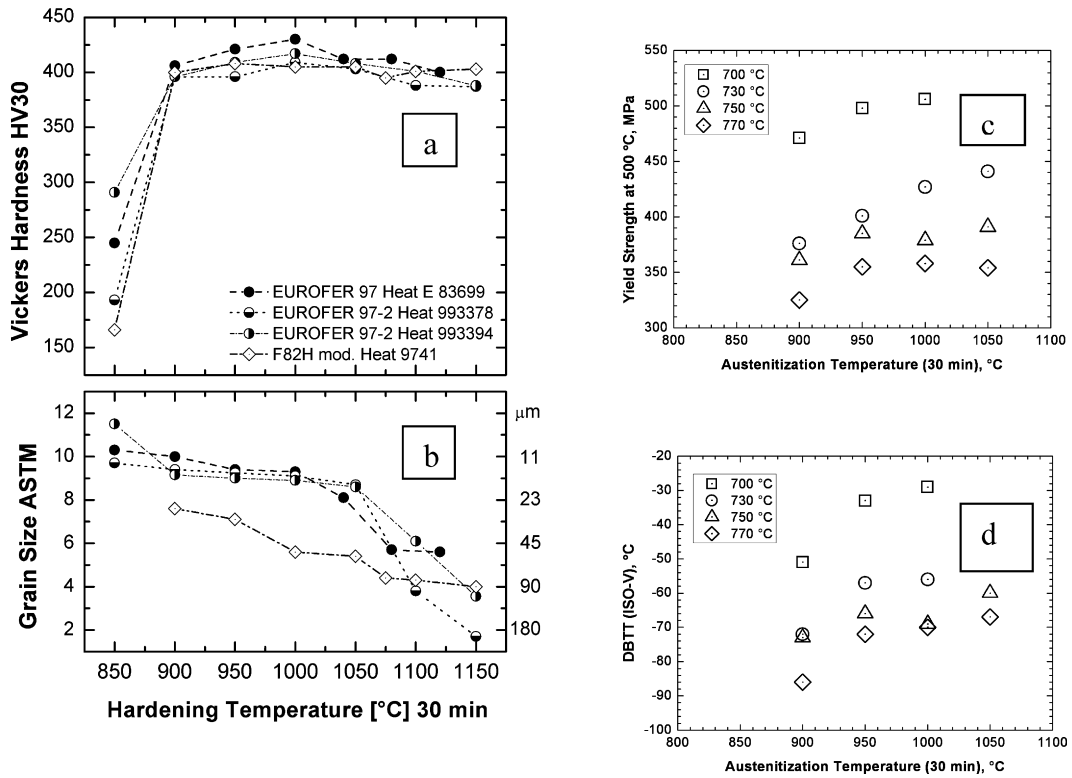


Fig. 4. RAFM steels: effect of heat – treatments on various properties. Effect of the austenitising temperature on (a) the hardness and (b) the grain-size (ASTM scale and real size in micrometers) [20]. Effect of the austenitising and tempering temperature on (c) the yield strength and (d) the Ductile-Brittle Transition Temperature (DBTT) measured by Charpy tests [21].

Fig. 4. Aciers ferritiques/martensitiques à activation réduite : effet des traitements thermiques sur différentes propriétés. Effet de la température d’austénitisation sur (a) la dureté et (b) la taille de grain (échelle ASTM et taille réelle en micromètre) [20]. Effet des températures d’austénitisation et de revenu sur (c) la limite d’élasticité et (d) la Température de Transition Ductile Fragile (TTDF) mesurée par essai Charpy [21].

Table 2

Typical chemical compositions of ODS ferritic steels in mass % [25,33,34]

Tableau 2

Compositions chimiques typiques d’aciers ODS ferritiques en % masse [25,33,34]

Element	12Y1	12YWT	14YWT	MA956	MA957	PM2000
C	0.045	0.05	0.036	0.03	0.030	0.01
N	0.017	0.014	0.140	0.029	0.044	0.0028
Cr	12.85	12.58	14.13	21.7	13.7	18.92
Si	0.03	0.18	0.030	0.05	0.04	0.04
W	< 0.01	2.44	1.94			0.04
V	0.007	0.002	0.010			
Mn	0.04	0.60	0.17	0.06	0.09	0.11
Ni	0.24	0.27	0.22	0.11	0.13	0.01
Mo	0.03	0.02	0.010	< 0.05	0.300	0.01
Al	0.007		0.000	5.77	0.03	5.1
Ti	0.003	0.35	0.22	0.33	0.98	0.45
Y	0.20	0.16	0.13	0.38	0.28	0.37
O	0.15	0.16	0.10	0.21	0.21	0.25
P	< 0.001	0.019		0.008	0.007	< 0.002
S	0.002	0.005	0.004	0.005	0.006	0.0021
B	0.004				0.0009	< 0.0003

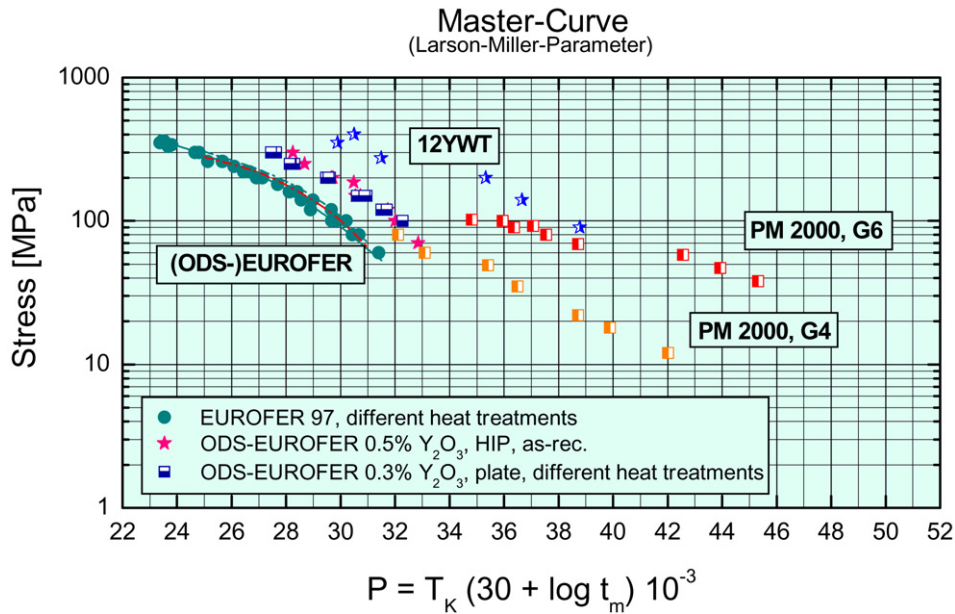


Fig. 5. Creep Rupture Strength for EUROFER, ODS EUROFER, the 12YWT ORNL development alloy, and, the industrial grade PM2000. PM2000 is tested in two metallurgical conditions: G6 with coarse grain (diameter in the mm range) and G4 with refined grains (diameter  $\sim 2$  to 10 micrometers) [25,26]. Times to rupture are represented versus the Larson–Miller parameter  $LM = T(30 + \log(t))$  where the temperature  $T$  is in Kelvin and the time to failure in hours.

Fig. 5. Résistance à la rupture en fluage de l'EUROFER, l'ODS-EUROFER, l'alliage de développement 12 YWT d'ORNL, et, la nuance industrielle PM2000. L'alliage PM2000 a été testé sous la forme de deux états métallurgiques qui diffèrent par leur taille de grain : G6 ayant un grain grossier (diamètre dans le domaine du mm) et G4 un grain plus fin (diamètre de  $\sim 2$  à 10 micromètres) [25,26]. Les temps à rupture sont représentés en fonction du paramètre de Larson–Miller  $LM = T(30 + \log(t))$  où la température est en Kelvin et le temps à rupture en heures.

which drive the system away from thermal equilibrium. This is a situation quite different to conventional metallurgy, where the microstructure and in-service properties of materials are tailored using pathways, which remain close to thermal equilibrium [35]. Stationary states, to which are brought driven systems under the MA process, have been shown, on particular systems, to be a function of temperature and a forcing parameter defined as the momentum transfer to the unit of mass of powder during the unit of time. Dynamical phase diagrams can be constructed with this type of forcing parameter, also called MA Intensity ( $I$ ), and, the temperature ( $T$ ): in this ( $I, T$ ) plane domains can be defined, where stationary phases are identified [36]. To our knowledge, this systematic driven alloy approach has not yet been used in the development of ODS steels.

High-energy MA of powder Fe–12.3wt%Cr–3%W–0.39%Ti, 0.25%Y<sub>2</sub>O<sub>3</sub>, typical of the 12YWT or Fe–14%Cr–3%W–0.4%Ti–0.3%Y<sub>2</sub>O<sub>3</sub> typical of 14YWT followed by hot extrusion at 1150 °C results in dissolving the Y<sub>2</sub>O<sub>3</sub> phase and forming a high number density  $\sim 10^{23}$  to  $10^{24}$  m<sup>-3</sup> of nano-clusters of average Guinier radius  $\sim 1$  nm as observed by Tomographic Atom Probe (TAP) [33,34]. Similar microstructures of nano-clusters are observed by TAP of MA957 [37]. These microstructures remain stable after creep up to 800 and 850 °C for 14,500 and 4000 hours, respectively [33,34]. These clusters are highly enriched in Y, Ti and O. The ratio (Y + Ti)at%/Oat% is close to one with significantly more Ti than Y, indicating that the nano-clusters were consistent with TiO rather than the original Y<sub>2</sub>O<sub>3</sub>, although Y<sub>2</sub>O<sub>3</sub> is more stable than any Ti oxide [38]. In addition, the Y and O levels in the ferrite matrix are found significantly higher than the equilibrium levels in  $\alpha$ -Fe (for instance  $< 7$  appm O in  $\alpha$ -Fe at 800 °C close to the extrusion temperature) [39], confirming the dissolution of yttria particles and the non-equilibrium state of the alloy. The role of the titanium seems to be important: for the 12Y1 experimental alloy with no Ti present, the same conditions of MA and hot extrusion as for 12YWT did not result in this dense population of nano-clusters but in a significantly lower number density  $\sim 10^{20}$ – $10^{21}$  m<sup>-3</sup> Y<sub>2</sub>O<sub>3</sub> particles with diameter in the range 10–40 nm [25].

The physical mechanisms governing the formation and the stability of the (Ti,Y)-O nano-clusters have still to be clarified. Small Angle Neutron Scattering (SANS) characterization carried out after MA confirmed the dissolution of the initial Y<sub>2</sub>O<sub>3</sub> and the formation of nano-clusters during various subsequent heat treatments [40]. The binding energy



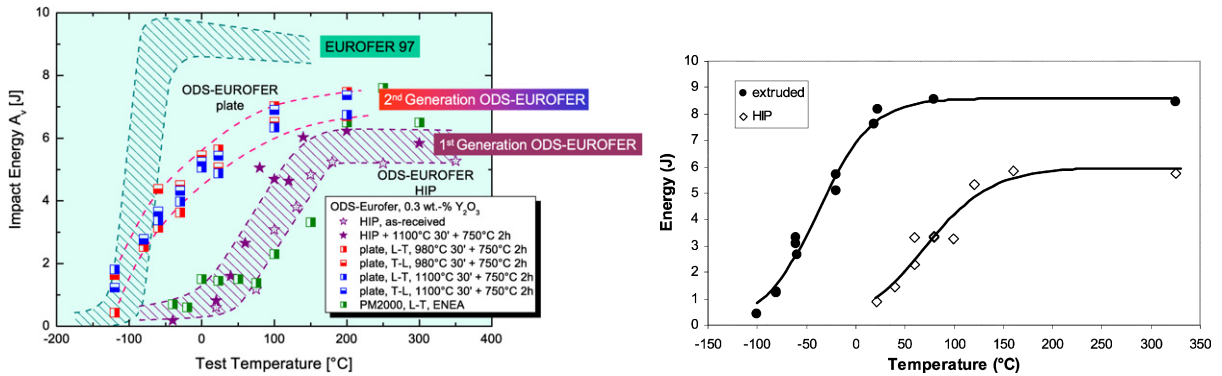


Fig. 6. (a) Impact energy of the first generation and second generation of ODS EUROFER. In the first generation the impact energies are affected by heavy carbide precipitation, that disappeared in the 2nd generation by appropriate thermal-mechanical treatment [30]. (b) Impact energy of ODS EUROFER fabricated starting from the same MA powder as in (a) but consolidated using either Hot Extrusion (extruded) or Hot Isostatic Pressing (HIP). Clearly hot extrusion process results in better fracture toughness [45].

Fig. 6. (a) Énergie Charpy de la première et de la deuxième génération d'ODS-EUROFER. Les énergies Charpy de la première génération sont affectées par une abondante précipitation de carbures, qui a disparu dans la deuxième génération grâce à un traitement thermo-mécanique approprié [30]. (b) Énergie Charpy d'un ODS-EUROFER fabriqué à partir de la même poudre broyée qu'en (a) mais consolidée soit par extrusion à chaud (extruded) soit par pressage isostatique à chaud (HIP). De toute évidence l'extrusion à chaud produit un matériau avec une bien meilleure ténacité [45].

between Ti and O atoms may play an important role, as a substantial fraction of the titanium and oxygen detected in TAP is in the form of  $TiO^{++}$  [34]. It should be noted that these nano-clusters do not seem to survive a hot extrusion at 1175 °C, as Tomographic Atom Probe does not reveal any of them after such a thermal mechanical treatment; instead, larger  $Y_2Ti_2O_7$  phases of average diameter  $\sim 20$  nm are observed within the grain by TEM diffraction contrast imaging [41].

Concerning the ODS EUROFER reinforced with yttrium oxide, High Resolution Transmission Electron Microscopy (HRTEM) revealed  $Y_2O_3$  particles with well-defined coherency relationship with the Fe–Cr matrix and mean diameter  $\sim 10$  nm [42]. Recent examination by TAP revealed that this material contains also a rather high density of oxygen and yttrium enriched clusters of mean diameter  $\sim 3$  nm [43].

The high creep strength is attributed to the dense population of nano-clusters described above. At intermediate temperatures the exponent of the stress in the Norton law expressing the strain rates is usually very high, greater than 10. This certainly indicates a high threshold stress for the dislocation to escape the nano-clusters, the origin of which requires many more creep experiments associated with dislocation structure observations. Nevertheless, this high strength is obtained at the expense of fracture toughness [30,44], although this remains significant. From a practical point of view, the anisotropy of the mechanical properties, the presence of inclusions and an optimized fabrication route are important issues to master for a reliable production and use of ODS steels. As shown in Fig. 6, both carbides and the process of the powder consolidation, Hot Isostatic Pressing (HIP) versus Hot Extrusion (HE), are important in mastering the fracture toughness and the DBTT [30,45]. Inclusions of carbide type, are also reported promoting cavitation and inducing brittle inter-granular creep failure in ODS ferritic steels [25].

In addition, welding is a critical issue, as conventional melting processes destroy the dispersion, resulting in joints with low strength. First trials on dissimilar diffusion welding, EUROFER/ODS-EUROFER have been successfully conducted [46]. First trials of the friction stir welding technique, successfully developed and used in the Aeronautics for Al alloys, are encouraging [47]. Research and Development are still needed for a reliable use of such techniques for nuclear components made of ODS steels.

## 5. Radiation effects

### 5.1. Simulating fusion specific radiation effects

In the absence of an irradiation facility with a prototypical neutron flux such as the International Fusion Materials Irradiation Facility (IFMIF) [48], irradiations have been conducted using fission reactors: Materials Testing Reactors (HFR-Petten, BR2 SCK·CEN/Mol, OSIRIS-CEA/Saclay, HFIR-Oak Ridge National Laboratory, SM2-Russia) or Fast

Breeder Reactors (Phénix-CEA/Marcoule, BOR60-Russia, Joyo-Japan) have been extensively used. The recovery stages of the point defects obtained after irradiation via fast fission and 14 MeV neutrons are the same [49]. Molecular Dynamics simulations have also shown that displacement cascades break down in sub-cascades of  $\sim 20$  keV for high recoil energies [11]. As a consequence, any irradiation effect of the 14 MeV neutrons, controlled by super-saturation and diffusion of point defects, can be confidently simulated using the fast spectra of fission reactors. Nevertheless, due to the shift of the PKA spectrum to higher energy, replacement sequences will be globally larger for the 14 MeV neutrons and specific effects on phase stability are not to be excluded [50].

In the absence of an intense 14 MeV neutron source several methods or tricks have been used to simulate the accumulation of point defects and He under fusion reactor relevant conditions. Boron or nickel doped steels were fabricated and irradiated in MTRs. However, these methods give questionable data. Due to its low solubility, boron is well known to segregate very easily to grain-boundaries so that the He (and Li) produced by the reaction  $^{10}\text{B}(n, \alpha)^7\text{Li}$  is not uniformly distributed. With Ni-doping, the two-stage reaction  $^{58}\text{Ni}(n, \gamma) \rightarrow ^{59}\text{Ni}(n, \alpha)$  is producing He. Nevertheless nickel strongly modifies the martensite transformation points and thus the microstructure and mechanical properties of the doped material in its initial metallurgical condition.  $^{54}\text{Fe}$  doped F/M steels are being fabricated and irradiated in MTR yielding a He/dpa ratio  $\sim 2$  appm/dpa. First results have been reported in [51]. He and H can also be produced with ratio to dpa typical of the D–T fusion spectrum by spallation nuclear reactions. Irradiations either under a 0.5–1 GeV proton beam [52] or in the mixed spallation-neutron spectrum of spallation target are used [53]. Nevertheless, spallation reactions produce also a complete range of residues from the atomic mass of the target nucleus down to H, which could have non-negligible impact on microstructure and properties, especially for high dose experiments. Finally, another method which has been extensively used is the implantation of energetic  $\alpha$  particles of energy in the range 20 to 100 MeV produced by cyclotron facilities. Using an energy degrader the He atoms can be uniformly implanted on thicknesses  $\sim 100$   $\mu\text{m}$ , allowing tensile testing and microstructure examination via Transmission Electron Microscopy (TEM) and Small Angle Neutron Scattering (SANS) [54,55]. The He/dpa ratio is typically  $\sim 6000$  appm/dpa.

### 5.2. Ferritic/martensitic steels: embrittlement and phase stability

The yield strength at low temperature of the ferritic and F/M steels is thermally activated due to the peculiar glide mechanisms of screw dislocations in the bcc crystalline structure [56]. As a consequence, below a critical temperature called the Ductile Brittle Temperature Transition (DBTT), the critical stress for cleavage is less than the yield strength, allowing the failure of the material via cleavage mechanisms i.e. separation of crystallographic planes thus with low energy instead of ductile failure with high failure energies. Any increase of the yield strength due to an increase of the strain rate or to radiation induced hardening, as well as a decrease of the cleavage stress due to any embrittlement mechanism during operation, will increase the DBTT.

The embrittlement created by displacement cascade damage of fission neutrons depends strongly on the irradiation temperature and on the chromium content as shown on Fig. 7. For irradiation temperatures above 380 °C, irradiation in Phénix induces a large increase of the DBTT shift within a 17%Cr ferritic steel associated with an intense  $\alpha/\alpha'$  unmixing, as for this Cr content and temperature, the alloy lies in the miscibility gap of the Fe–Cr system. For the 9%Cr–1Mo steels negligible  $\alpha/\alpha'$  unmixing was detected and the radiation induced embrittlement is limited [16]. For irradiation temperature close to 325 °C significant embrittlement is measured for the conventional 9Cr1Mo and for EUROFER [57]. The contribution of  $\alpha/\alpha'$  unmixing is not excluded at this temperature, even with 9% Cr content. Increasing  $\alpha'$  volume fraction was detected by SANS in RAFM steels with increasing Cr content above  $\sim 7$ –7.5%Cr irradiated in OSIRIS at 325 °C up to 0.7 dpa [58]. Microstructure examination, more realistic phase diagram and appropriate kinetics tools [59] will allow us to better understand the phase instability contribution to this low temperature embrittlement.

### 5.3. Ferritic/martensitic steels: helium induced hardening and embrittlement

Uniform implantation of high energy alpha particles of energy in the range 20 to 100 MeV has been proven particularly effective in studying induced microstructure and tensile properties under well controlled and versatile conditions of flux and temperature [54,55]. As shown in Fig. 8 the implantation of He at 250 °C clearly results in an important hardening and nearly complete loss of ductility for He content above  $\sim 2500$  appm He. TEM examined

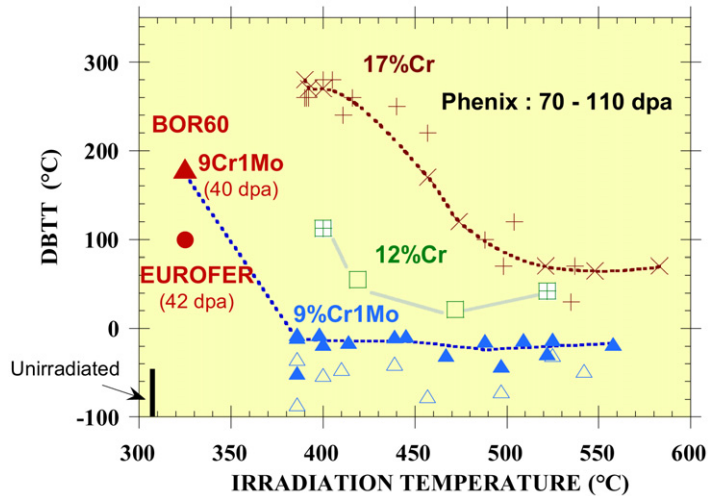


Fig. 7. Effect of the irradiation temperature on the DBTT for a ferritic steel (17%Cr), conventional 12%Cr and 9%Cr1Mo ferritic/martensitic steels and EUROFER. For irradiation temperatures close to 320 °C and above 380 °C data have been obtained after irradiation in BOR60 [57,61] and Phénix [16] respectively.

Fig. 7. Effet de la température d'irradiation sur la Température de Transition Ductile Fragile (TTDF) d'un acier ferritique (17 %Cr) et d'aciers ferritiques/martensitiques à 12%Cr, 9Cr1Mo ou EUROFER. Pour les températures d'irradiation proches de 320 °C ou au-dessus de 380 °C les données ont été obtenues dans BOR60 [51,61] et Phénix [16] respectivement.

microstructure of samples implanted at 250 and 550 °C consists in He clusters or bubbles as shown in Figs. 8(c) and 8(d), respectively [55]. The hardening that can be deduced using an Orowan model is in good qualitative agreement with the measured hardening [56]. An important question is the following: is this hardening sufficient to promote the inter-granular failure along the prior austenite grain boundaries, as observed experimentally? The answer is most probably, no: the same heat of modified 9Cr 1Mo irradiated in a quenched martensite initial condition exhibits very similar yield strength  $\sim 1200$  MPa after irradiation in OSIRIS at 320 °C up to  $\sim 3$  dpa [55], but fails under tensile tests with transgranular failure surface.

In conclusion, the implantation of alpha particles at low temperature down to  $\sim 250$  °C results in a large hardening of material, with a significant weakening of the prior austenitic grain-boundaries, although no He-bubbles along these boundaries have been observed using TEM examination. A large data base of mechanical properties of neutron irradiated F/M steels under various spectra including spallation spectrum, where up to  $\sim 100$  appm He/dpa are produced, has been analyzed, showing that above a content of He situated at  $\sim 500$  appm, hardening is associated with the occurrence of inter-granular embrittlement [60].

It is not the first time that metallurgy is facing an embrittlement issue due to possible segregation of an impurity into planar defects. The solution is to try to get the impurity trapped within the grain. For steel-makers it was the historical cases of oxygen and sulfur, which are now commonly trapped in alumina and manganese sulfides. For He, the solution has to be found in selecting the most effective traps, carbides or dislocations for example, to keep He within the grain. In this future work, determining the energetics of He in presence of these objects will be of prime importance. On this basis, kinetic tools able to describe diffusion and clustering of He in the grains and grain-boundaries will guide the optimization of the microstructure.

#### 5.4. ODS Ferritic steels: grain size and embrittlement

MA957, which has the dense dispersion of nano-clusters revealed by TAP and assumed to control the high heat resistance [37], was irradiated in BOR60 up to  $\sim 30$  dpa, in two metallurgical conditions: (i) hot-extruded and stress-relieved at 920 °C, which resulted in fine elongated grains of diameter  $\sim 0.5$  micrometers, and (ii) hot-extruded and recrystallized at 1100 °C, resulting in grain diameters in the range 20–50 micrometers. Both materials exhibit similar radiation hardening, the sub-micronic grain material having yield strength  $\sim 500$  MPa higher than the recrystallized batch. Nevertheless the fine-grained batch retains total elongation (7%) and reduction of area (41%), half the initial

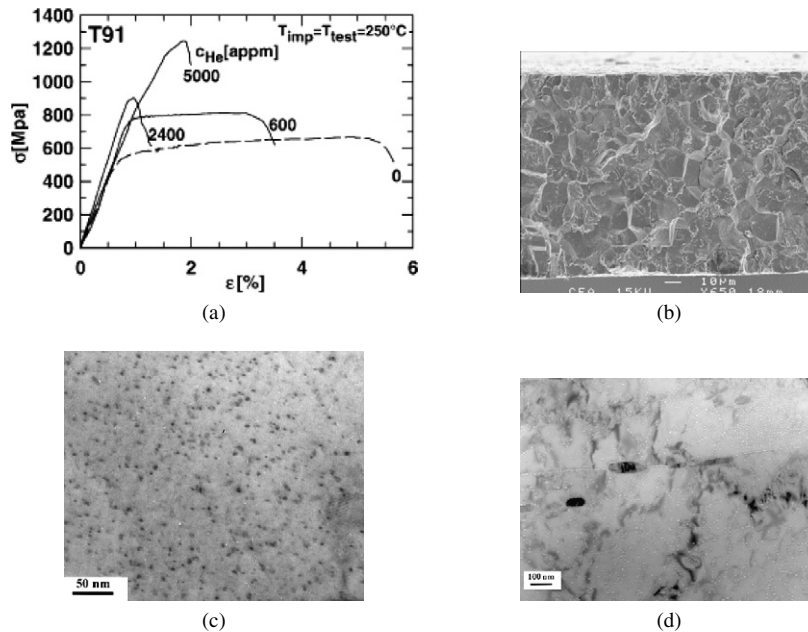


Fig. 8. (a) Tensile behaviour of modified 9%Cr–1Mo after uniform implantation of 23 MeV  $\alpha$ -particles up to a maximum of 5000 appm at 250 °C carried out at the compact cyclotron of Forschungszentrum Jülich (FZJ) [54]. (b) Intergranular fracture surface after implantation at of 5000 appm He 250 °C along the prior austenite grains observed by Scanning Electron Microscopy (SEM). (c) TEM observation of He–V nano-clusters in samples implanted at 250 °C up to 5000 appm He [55]. (d) TEM observation of He–V bubbles along dislocations and interfaces in samples implanted at 550 °C up to 5000 appm He [55]. For 5000 appm He the dose is  $\sim 0.8$  dpa.

Fig. 8. (a) Comportement en traction d'un acier à 9%Cr–1Mo après implantation uniforme de particules  $\alpha$  de 23 MeV jusqu'à un maximum de 5000 ppm atomiques à 250 °C au cyclotron du Forschungszentrum Jülich (FZJ) [54]. (b) Surface de rupture intergranulaire le long des anciens joints de grains austénitiques observée au Microscope Électronique à Balayage (MEB) après implantation de 5000 ppm atomiques d'He à 250 °C. (c) Observation au Microscope Electronique à Transmission (MET) d'amas d'He et de lacunes dans un échantillon avec 5000 ppm atomiques d'He implantées à 250 °C [55]. (d) Observation au MET d'amas d'He et de lacunes dans un échantillon avec 5000 ppm atomiques d'He implantées à 550 °C [55]. Pour 5000 ppm atomiques la dose est  $\sim 0.8$  dpa.

values: this indicates that the initial fracture toughness is hardly affected, whereas the coarse-grained batch should suffer of a severe loss of fracture toughness with total elongation and reduction of area close to zero after irradiation [61].

The microstructure of these samples is still to be characterized to obtain data about the stability of the nano-cluster dispersion and the  $\alpha/\alpha'$  unmixing. Up to now most of the studies of the radiation stability of the oxide dispersion have been carried out with TEM and concerned oxide particles rather than the nano-clusters revealed by TAP (see for instance reference [62]). To our knowledge, only reference [63] reported, based on TAP examination, on the stability of the nano-clusters of the 12YWT alloy after irradiation with 150 keV Fe ion irradiation up to 0.7 dpa at 300 °C.

These microstructure investigations are essential to assess the viability of the grades with sub-micronic grain-size for a reasonable compromise between radiation hardening and fracture toughness of ODS steels. In addition, it can be seen, Fig. 5, that decreasing the grain diameter in the PM2000 type of ODS ferritic steel, decreases also the creep strength at high temperature, showing that a trade-off on the grain-size should be found between high fracture toughness and creep strength.

### 5.5. Ferritic and ferritic/martensitic steels: the issue of radiation hardening saturation

Settling the issue of the saturation of the radiation induced hardening and embrittlement with dose is of high practical importance as it can save funding by giving an upper limit to the irradiation dose range to explore. It also greatly simplifies the structural assessment of highly irradiated components. Fig. 9 shows the European results obtained in OSIRIS (1–9 dpa), SM2 (8–14 dpa) and BOR 60 (32–42 dpa) and gathered in references [57,61]. It can be seen that, on the pure empiricism approach followed here, it is quite impossible to settle this issue of radiation hardening sat-

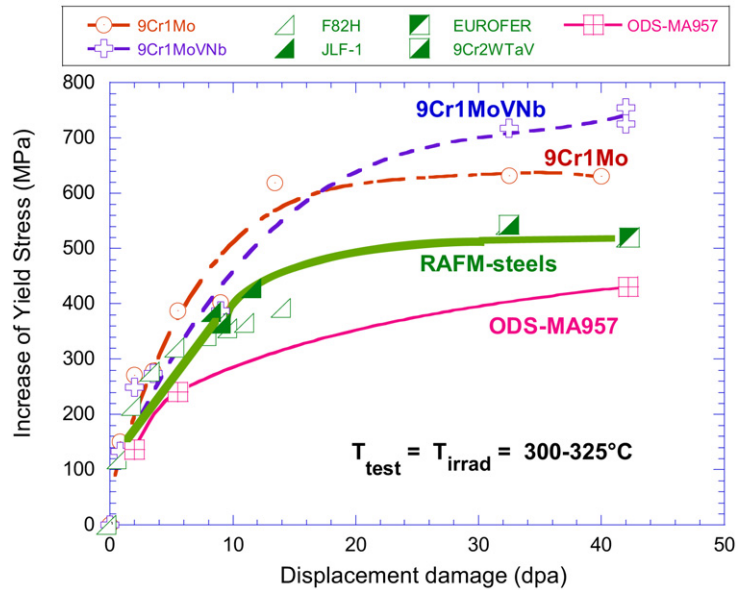


Fig. 9. Radiation induced hardening measured by the increase of the yield stress for (i) various conventional 9 Cr steels: 9Cr–1Mo and modified 9Cr–1Mo (9Cr1MoVNb), (ii) RAFM steels: F82H, JLF-1, EUROFER, 9Cr2WTa, (iii) ODS steel MA957 [57,61].

Fig. 9. Durcissement d’irradiation mesuré par l’augmentation de la limite d’élasticité pour (i) divers aciers conventionnels à 9 %Cr : 9Cr–1Mo et 9Cr–1Mo modifié (9CrMoVNb), (ii) aciers à activation réduite : F82H, JLF-1, EUROFER, 9Cr2WTa, (iii) acier ODS MA957 [57,61].

uration with dose. In addition, the hardening of ODS steels is significantly lower than in the F/M steels obtained by classical metallurgy, although ODS steels have higher initial yield strength. This might be due to the high density of nano-clusters, which could favor elimination and/or recombination of point defects.

### 5.6. Radiation-effect in $\text{SiC}_f/\text{SiC}$ composites

Silicon carbide composites were initially developed for aerospace and fossil energy applications for which high temperature strength, strength to mass ratio, and corrosion resistance are the most important properties controlling system design and performance. Due to high strength at high temperature, Silicon carbide (SiC) could make possible a direct He-cooled concept for fission reactors [3]. SiC is also attractive for fusion reactors. It should allow TBB concepts with high thermal efficiency made of a low activation structural material.

Silicon carbide exists under numerous crystalline polytypes of cubic or hexagonal crystalline structures. Whatever the polytype is, radiation effects are important with: (i) amorphisation at low temperature below typically  $\sim 200^\circ\text{C}$ , (ii) point-defect swelling regime up to  $\sim 1200^\circ\text{C}$ , and finally (iii) a void swelling regime above  $\sim 1200^\circ\text{C}$  [64]. Monolithic SiC, being a semi-conductor with large gap [65], post-irradiation thermal conductivity is controlled by phonons. Radiation defects clearly control the lattice thermal conductivity. Strong reduction has been measured at room temperature from initial values of  $\sim 370\text{ W/mK}$  down to saturation value  $\sim 10\text{ W/mK}$  after irradiation in the range  $300$  to  $800^\circ\text{C}$  beyond  $10\text{ dpa}$  [66].

Monolithic SiC is a rather brittle material with DBTT temperatures as high as  $1000$ – $1100^\circ\text{C}$  for usual strain-rate in the range  $10^{-6}$  to  $10^{-4}\text{ s}^{-1}$  in the case of a 4H–SiC hexagonal polytype [67]. This aspect has been the driving force for the development of composites consisting of SiC fibers, SiC matrix and interphases between the fibre and the matrix. The development of cubic  $\beta$ -SiC fibres, nearly stoichiometric and with low O content, has allowed to one developing  $\text{SiC}_f/\text{SiC}$  composites with rather high stability of mechanical strength and strain to failure for doses at least up to  $10\text{ dpa}$  [68].

Nevertheless, several issues should be solved for an engineering use of  $\text{SiC}_p/\text{SiC}$  composite in fusion or Gen IV reactors. Following the engineering experience gained from the metallic cladding of the fuel elements of the fast breeder reactors the usually rather low strain to failure of the  $\text{SiC}_f/\text{SiC}$  composites has to be improved and maintained after irradiation at least in the range of a few  $10^{-3}\text{ m/m}$ . The tightness of this type of material is also poor and coating

stable under irradiation and mechanical loading are to be developed and tested. Finally, joining these materials remains an open issue.

## 6. Conclusion and perspectives

High radiation resistant structural materials for the fusion and fission NPPs are a key issue for the development of both types of reactors.

Ferritic/martensitic steels have been selected on the basis of the experience gained from the various fast reactor development programmes of the last century. They are suffering at low temperature from embrittlement triggered by helium: intergranular failure along the prior austenitic grains is promoted, although no grain-boundary He-bubbles are observed using TEM. In addition, the contribution of  $\alpha/\alpha'$  unmixing to the hardening and embrittlement is not to be excluded. The kinetics of the hardening and embrittlement versus dose, especially saturation with dose is still a key open issue of prime importance for the assessment the structural integrity of the future components. We have shown as well the progress that has been achieved and is still to be made to master the initial microstructure, inclusion cleanness and joining techniques of ODS steels for higher heat resistance.

It should be noted that the experimental data shown in this paper have been obtained during the past forty years. It is a lengthy process that is triggered by the duration of irradiation and in hot cell testing. Typically, obtaining post-irradiation data after  $\sim 40$  dpa within a fast reactor requires  $\sim 4$  years. As a consequence, the experimental feedback for material development is a process spread over long time periods if only this purely empirical approach based on neutron irradiation is used.

Using ion beam irradiation, a versatile and reliable technique with rapid feedback, physical understanding of radiation effects at the atomic scale has also been achieved during these past forty years [49]. In parallel, the progress made in the ab initio calculations showed that physically based multi-scale modeling is possible, at least for simple systems [69]. On this basis, fusion and fission material development programmes were including the development of physically based modeling in order to capture the physics of radiation effects at the relevant scales within systems encompassing the most significant aspects of real industrial alloys [70]. It is clear that the progress made up to now and presented in this issue will greatly renew the development of radiation resistant materials, improving their phase stability prediction and optimizing their microstructure.

On the longer term these experimentally validated and physically based modeling tools should be essential for: (i) extrapolating the data obtained within various spectra to the actual one, especially in the case of fusion, (ii) optimizing neutron irradiation programs to qualify materials under prototypical spectrum such as in IFMIF, the future intense source of 14 MeV neutrons [48], and (iii) reliably extrapolating the qualification data bases to the larger operating conditions of reactors.

Finally, for a safe and economic operation of the future fusion and fission NPPs, components made of these structural materials with increased radiation resistance will have to be developed, tested and their integrity assessed. Here again, physically based modeling should provide guidance to improve the realism of the constitutive laws and damage rules used in the present codes [71].

## Acknowledgements

We would like to acknowledge our colleagues of the EFDA-CSU Garching, especially R. Laesser and E. Diegele, of CEA, N. Chauvin and J.L. Séran and all the researchers of the EU Material Development programme for fruitful discussion and remarks.

## References

- [1] P. Norajitra, L. Bühler, A. Buenaventura, E. Diegele, U. Fischer, E. Hutter, R. Kruessmann, S. Malang, J. Reimann, A. Orden, D. Ward, G. Vieider, F. Wasatjerna, Conceptual design of the dual-coolant blanket in the frame of the EU power plant conceptual study, FZKA Report 6780, November 2002.
- [2] Generation IV International Forum: <http://www.gen-4.org>.
- [3] N. Chauvin, J.C. Garnier, J.L. Séran, Ph. Brossard, in: Proceedings of the International Congress on Advances in Nuclear Power Plants, ICAPP-03, May 4–7 2003, Paper 3339, Cordoba, Spain.
- [4] K. Ehrlich, Philos. Trans. Roy. Soc. London Ser. A 357 (1999) 595–623.

- [5] P. Norajitra, L.V. Boccaccini, A. Gervash, R. Giniyatulin, N. Holstein, T. Ihli, G. Janeschitz, W. Krauss, R. Kruessmann, V. Kuznetsov, A. Makhankov, I. Mazul, A. Moeslang, I. Ovchinnikov, M. Rieth, B. Zeep, *J. Nucl. Mater.* 367–370 (2007) 1416–1421.
- [6] M. Faleschini, H. Kreuzer, D. Kriener, R. Pippan, *J. Nucl. Mater.* 367–370 (2007) 800–805.
- [7] Ph. Martin, N. Chauvin, J.C. Garnier, M. Masson, Ph. Brossard, P. Anzieu, in: *Proceedings of the 7th International Conference GLOBAL 2005*, organised by the Atomic Energy Society of Japan (AESJ), Tsukuba, Ibarakiken, Japan, Paper 327.
- [8] Matériaux pour le réacteur à très haute température, *Les Réacteurs Nucléaires à Caloporteur Gaz*, Monographie de la Direction de l'énergie nucléaire, CEA, Editions Le Moniteur, pp. 33–44 and 45–48.
- [9] A.A. Tavassoli, *J. Nucl. Mater.* 155–157 (1988) 105–112.
- [10] Matériaux pour le réacteur à très haute température, *Les Réacteurs Nucléaires à Caloporteur Gaz*, Monographie de la Direction de l'énergie nucléaire, CEA, Editions Le Moniteur, pp. 77–83.
- [11] P. Vladimirov, S. Bouffard, *C. R. Physique* 9 (3–4) (2008) 303–322.
- [12] R. Schaeublin, J. Henry, Y. Dai, *C. R. Physique* 9 (3–4) (2008) 389–400.
- [13] L.K. Mansur, E.H. Lee, *J. Nucl. Mater.* 179–181 (1991) 105–110.
- [14] M.J. Caturla, et al., Helium and point defect accumulation: (ii) kinetic modelling, *C. R. Physique* 9 (3–4) (2008) 401–408.
- [15] J.L. Boutard, in: *Proceedings 43th Colloque de Métallurgie de l'INSTN*, *J. Physique* IV 11 (Pr1) (2001) 187–201.
- [16] J.L. Séran, A. Alamo, A. Maillard, H. Touron, J.C. Brachet, P. Dubuisson, O. Rabouille, *J. Nucl. Mater.* 212–215 (1994) 588–593.
- [17] R. Lindau, A. Möslang, M. Rieth, M. Klimiankou, E. Materna-Morris, A. Alamo, A.A. Tavassoli, C. Cayron, A.M. Lancha, P. Fernandez, N. Baluc, R. Schaeublin, E. Diegele, G. Filacchioni, J.W. Rensman, B. van der Schaaf, E. Lucon, W. Dietz, *Fusion Eng. Design* 75–79 (2005) 989–996.
- [18] (a) A.A. Tavassoli, A. Alamo, L. Bedel, L. Forest, J.M. Gentzittel, J.W. Rensman, E. Diegele, R. Lindau, M. Schirra, R. Schmitt, H.C. Schneider, C. Petersen, A.M. Lancha, P. Fernandez, G. Filacchioni, M.F. Maday, K. Mergia, N. Boukos, N. Baluc, P. Spätig, E. Alves, E. Lucon, *J. Nucl. Mater.* 329–333 (2004) 257–262;  
(b) B. van der Schaaf, E. Diegele, R. Laesser, A. Möslang, *Fusion Eng. Design* 81 (2006) 893–900.
- [19] W. Hume-Rothery, *The Structures of Alloys of Iron: An Elementary Introduction*, first ed., Pergamon Press, 1966.
- [20] L. Schaefer, M. Schirra, K. Ehrlich, *J. Nucl. Mater.* 233–237 (1996) 263–269.
- [21] M. Rieth, private communication.
- [22] J. Nutting, The long term structural stability of power generation steels – some basic considerations, in: *Proceedings of the Conference on Advanced Heat Resistant Steels for Power Generation*, San Sebastian, Spain, April 27–29, 1998, Cambridge University Press, Cambridge, 1998.
- [23] F. Masuyama, New developments in steels for power generation boilers, in: *Proceedings of the Conference on Advanced Heat Resistant Steels for Power Generation*, San Sebastian, Spain, April 27–29, 1998, Cambridge University Press, Cambridge, 1998.
- [24] A. Czyska-Filemonowicz, B. Dubiel, *J. Mater. Technol.* 64 (1997) 53–64.
- [25] R.L. Klueh, J.P. Shingledecker, R.W. Swindeman, D.T. Hoelzer, *J. Nucl. Mater.* 341 (2005) 103–114.
- [26] R. Lindau, A. Alamo, Private communication.
- [27] J.-J. Huet, H. Massaux, L. De wilde, J. Moels, *Rev. Métall.* 65 (1968) 12.
- [28] S. Ukai, T. Nishida, H. Okada, T. Okuda, M. Fujiwara, K. Asabe, *J. Nucl. Sci. Technol.* 34 (1997) 256.
- [29] S. Ukai, T. Yoshitake, S. Mizuta, Y. Matsudaira, S. Hagi, T. Kobayashi, *J. Nucl. Sci. Technol.* 36 (1999) 710.
- [30] M. Klimiankou, R. Lindau, A. Moeslang, *J. Nucl. Mater.* 367–370 (2007) 173–178.
- [31] A. Alamo, V. Lambard, X. Averty, M.H. Mathon, *J. Nucl. Mater.* 329–333 (2004) 333–337.
- [32] D.K. Mukhopadhyay, F.H. Froes, D.S. Gelles, *J. Nucl. Mater.* 258–263 (1998) 209.
- [33] M.K. Miller, E.A. Kenik, K.F. Russell, L. Heatherly, D.T. Hoelzer, P.J. Maziasz, *Mater. Sci. Eng. A* 353 (2003) 140.
- [34] M.K. Miller, K.F. Russell, D.T. Hoelzer, *J. Nucl. Mater.* 351 (2006) 262–268.
- [35] P. Bellon, R.S. Averback, *Scripta Mater.* 49 (2003) 921–925.
- [36] P. Pochet, E. Tominez, L. Chaffron, G. Martin, *Phys. Rev. B* 52 (3) (1995) 4006–4016.
- [37] M.K. Miller, D.T. Hoelzer, E.A. Kenik, K.F. Russell, *J. Nucl. Mater.* 329–333 (2004) 338–341.
- [38] D.R. Sigler, *Oxid. Met.* 32 (5–6) (1989) 337.
- [39] J.H. Swisher, E.T. Turkdogan, *Trans. Met. Soc. AIME* 239 (1967) 426.
- [40] M.J. Alinger, G.R. Odette, D.T. Hoelzer, *J. Nucl. Mater.* 329–333 (2004) 382–386.
- [41] D.T. Hoelzer, J. Bentley, M.A. Sokolov, M.K. Miller, G.R. Odette, M.J. Alinger, *J. Nucl. Mater.* 367–370 (2007) 166–172.
- [42] M. Klimiankou, R. Lindau, A. Moeslang, *J. Nucl. Mater.* 329–333 (2004) 347–351.
- [43] P. Vladimirov, A. Moeslang, R. Lindau, M. Klimenkov, C. Eisel, R. Coppola, A.A. Aleev, A.V. Karpov, O.N. Makeev, S.V. Rogozhkin, A.G. Zaluzhnyi, *Workshop on Structural Materials for Innovative Nuclear Systems (SMINS)*, FZ-Karlsruhe June 4–6, 2007.
- [44] M.A. Sokolov, D.T. Hoelzer, R.E. Stoller, D.A. Mcclintock, *J. Nucl. Mater.* 367–370 (2007) 213–216.
- [45] A. Alamo, A. Bougault, Contribution to the Fusion EURATOM programme TW5-TTMS006, Private communication.
- [46] R. Lindau, M. Klimiankou, A. Möslang, A. Rieth, B. Schedler, J. Schröder, A. Schwaiger, in: *Proceedings of the 16th International Plansee Seminar*, vol. 1: High Performance Powder Metallurgy Materials, Reutte, Austria, May 30–June 3, 2005, Plansee AG, Reutte, 2005, pp. 545–5557.
- [47] P. Miao, G.R. Odette, J. Gould, J. Bernath, R. Miller, M. Alinger, C. Zanis, *J. Nucl. Mater.* 367–370 (2007) 208–212.
- [48] A. Möslang, IFMIF: the intense neutron source to qualify materials for fusion reactors, *C. R. Physique* 9 (3–4) (2008) 457–468.

- [49] A. Barbu, Modelling of long term kinetic evolution: a fruitful relationship between experiment and theoretical development, C. R. Physique 9 (3–4) (2008) 353–361.
- [50] G. Martin, P. Bellon, Radiation effects in concentrated alloys and compounds: equilibrium and kinetics of driven systems, C. R. Physique 9 (3–4) (2008) 323–334.
- [51] D.S. Gelles, M.L. Hamilton, B.M. Oliver, L.R. Greenwood, S. Ohnuki, K. Shiba, Y. Kohno, A. Kohyama, J.P. Roberston, J. Nucl. Mater. 307–311 (2002) 212–216.
- [52] R. Schaeublin, M. Victoria, J. Nucl. Mater. 283–287 (2000) 339–343.
- [53] Y. Dai, P. Marmy, J. Nucl. Mater. 343 (2005) 247–252.
- [54] J. Henry, M.H. Mathon, P. Jung, J. Nucl. Mater. 318 (2003) 249–259.
- [55] P. Jung, J. Henry, J. Nucl. Mater. 318 (2003) 241–248.
- [56] D. Rodney, Atomic modeling of irradiation-induced hardening, C. R. Physique 9 (3–4) (2008) 418–426.
- [57] A. Alamo, J.L. Bertin, V.K. Shamardin, P. Wident, J. Nucl. Mater. 367–370 (2007) 54–59.
- [58] M.H. Mathon, Y. de Carlan, G. Geoffroy, X. Averty, A. Alamo, C.H. de Novion, J. Nucl. Mater. 312 (2003) 236–248.
- [59] D. Nguyen-Manh, et al., The Fe–Cr system: atomistic modeling of thermodynamics and kinetics of phase transformations, C. R. Physique 9 (3–4) (2008) 379–388.
- [60] T. Yamamoto, G.R. Odette, H. Kishimoto, J.W. Rensman, P. Miao, in: 7th International Workshop on Spallation Materials Technology (IWSMT-7), J. Nucl. Mater. 356 (1–3) (15 September 2006) 27–49.
- [61] A. Alamo, P. Wident, V. Shamardin, Final Report TW2-TTMS-001-D02: CEA REPORT DMN/SRMA/NT/2006-2767/A.
- [62] I. Monnet, P. Dubuisson, Y. Serruys, M.O. Ruault, O. Kaitasov, B. Jouffrey, J. Nucl. Mater. 336 (2004) 311–321.
- [63] P. Pareige, M.K. Miller, R.E. Stoller, D.T. Hoelzer, E. Cadet, B. Radiguet, J. Nucl. Mater. 360 (2007) 136–141.
- [64] E.E. Bloom, J. Nucl. Mater. 258–263 (1998) 7–17.
- [65] Ch. Kittel, Introduction to Solid States Physics, third ed., John Wiley and Sons, Inc., New York, 1966.
- [66] L.L. Snead, J. Nucl. Mater. 329–333 (2004) 524–529.
- [67] J.-L. DemeNET, M.H. Hong, P. Pirouz, Scripta Mater. 43 (9) (2000) 865–870.
- [68] R.H. Jones, L. Giancarli, A. Hasegawa, Y. Katoh, A. Kohyama, B. Riccardi, L.L. Snead, W.J. Weber, J. Nucl. Mater. 307–311 (2002) 1057–1072.
- [69] See for instance in Current Opinion in Solid State and Materials Science 3 (1998):
- (a) E. Kaxiras, S. Yip, Modelling and simulation of solids 523–525.
  - (b) R. Phillips, Modelling in the mechanics of materials 526–532.
  - (c) G. Martin, Modelling materials driven far from equilibrium 552–557.
- [70] (a) M. Victoria, S. Dudarev, J.L. Boutard, E. Diegele, R. Lässer, A. Almazouzi, M.J. Caturla, C.C. Fu, J. Källne, L. Malerba, K. Nordlund, M. Perlado, M. Rieth, M. Samaras, R. Schaeublin, B.N. Singh, F. Willaime, Fusion Eng. Design 82 (2007) 2413–2421;
- (b) P. Ledermann, J.L. Boutard, M. Guttmann, B. Marini P. Garcia, C. Valot, La Revue de Métallurgie-CIT Novembre, 2005, pp. 917–930.
- [71] M. Samaras, W. Hoffelner, M. Victoria, J. Nucl. Mater. 371 (2007) 28–36.